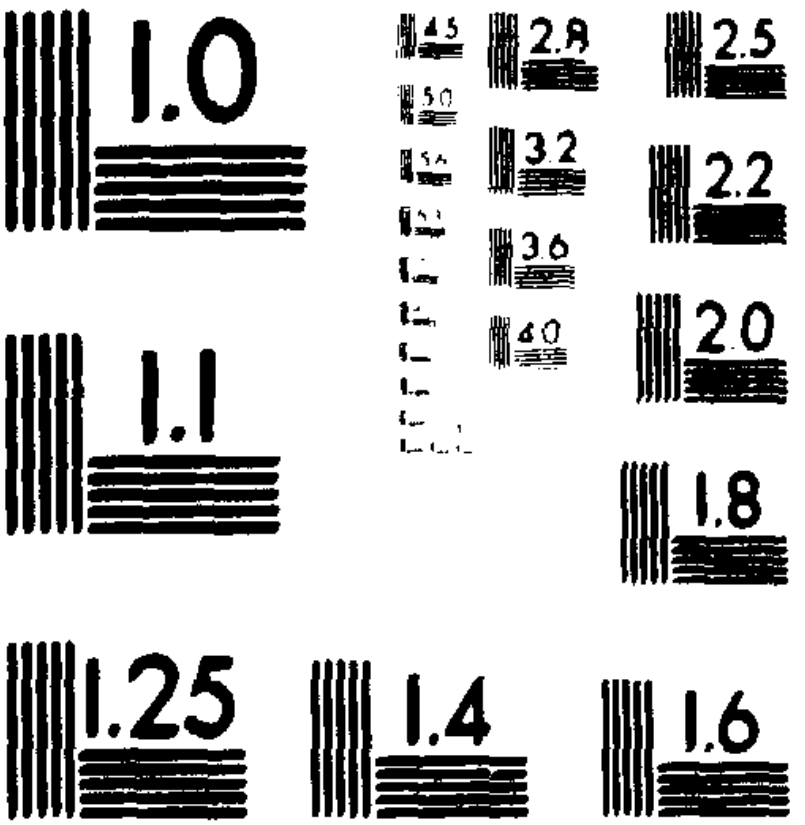

ISSN/0393-6287

RT/FUS/86/1

CONTRIBUTIONS TO THE 7th INTERNATIONAL CONFERENCE ON PLASMA-SURFACE INTERACTIONS IN CONTROLLED FUSION DEVICES (Princeton, 5-9 May 1986)

COMITATO NAZIONALE PER LA RICERCA E PER LO SVILUPPO DELL'ENERGIA NUCLEARE E DELLE ENERGIE ALTERNATIVE

ISSN/0393-6287

COMITATO NAZIONALE PER LA RICERCA E PER LO SVILUPPO
DELL'ENERGIA NUCLEARE E DELLE ENERGIE ALTERNATIVE
ASSOCIAZIONE EURATOM-ENEA SULLA FUSIONE

CONTRIBUTIONS TO THE 7th INTERNATIONAL CONFERENCE ON PLASMA-SURFACE INTERACTIONS IN CONTROLLED FUSION DEVICES (Princeton, 5-9 May 1986)

ENEA-Dipartimento Fusione, Centro ricerche energia Frascati

RT/FUS/86/1

Testo pervenuto nel maggio 1986

This report has been prepared by: Servizio Studi e Documentazione - ENEA, Centro Ricerche Energia Frascati, C.P. 65 - 00044 Frascati, Rome, Italy.

This Office will be glad to send further copies of this report on request.

CONTENTS

ENERGY LOSSES IN NORMAL FT (FRASCATI TOKAMAK) DISCHARGES

G. Maddaluno, M. Ciotti*, C. Ferro

Associazione EURATOM-ENEA sulla Fusione, Centro Ricerche Energia Frascati
C.P. 65 - 00044 Frascati, Rome (Italy)

A systematic analysis of the temperature increase of the limiter and wall in FT has been performed using thermocouples to calculate power losses during normal discharges. A linear increase of the total power to the limiter was found ranging from 10% of the total input power at $n_e = 0.3 \cdot 10^{14}$ cm^{-3} up to 35% at $n_e = 3.10^{14}$ cm^{-3}. The power lost to the wall was of the order of 70% increasing if the electron density is increased with higher plasma current. The overall energy balance tends to 100% at higher current and density ($n_e > 1 \cdot 10^{14}$ cm^{-3}) suggesting a more uniform distribution of the energy fluxes. A characteristic decay length of the energy ranging from 0.5 to 1 cm was also estimated.

---

* ENEA Guest

1. INTRODUCTION

Knowledge of the actual heat fluxes incident on exposed surface has become increasingly important for the design of vacuum vessels and limiters in future devices.

A systematic analysis in the FT device is being carried out in order to obtain information about energy loss channels from thermal load measurements on the limiter and the vacuum chamber.

The geometry of the FT does not allow the possibility of performing surface thermography of exposed surfaces.

Two sets of thermocouples were used for measuring temperature increase of the linear and of two parts of the main poloidal limiter. The shape of the temperature versus the time curve was analyzed for information on scrape-off parameters and the power flux to the limiter and liner.

Section 2 describes the experimental layout; sect. 3 reports and discusses the experimental maximum temperature increases obtainded on numerous discharges (~ 200) with a large variety of parameters; sect. 4 a simple power balance picture of a representative group of discharges (40) is reported and discussed.

2. EXPERIMENTAL DESCRIPTION

A general view of the FT vacuum chamber is shown in Fig. 1.

Starting from the inside, there is an inner vacuum chamber (a stainless steel bellows of thickness 0.04 cm), a copper shell, and an outer vacuum vessel (a stainless steel bellow).

The walls of the first vacuum chamber are protected by safety rings (minor radius 22.4 cm) and a main poloidal limiter which can be inserted or removed without having to open the vacuum vessel [1].

The main limiter consists of two half rings which are electrically insulated with respect to the vacuum vessel and to each other.

Several limiters having different geometries have been tested [1]. Since May 1983 the limiter consists of two half rings of stainless steel (AISI 316) supporting 38 mushroom-shaped pieces made either in stainless steel [2] or in Inconel 600.

On the rear surface of the inner vacuum bellows four thermocouples are located at about 180° toroidally from the main limiter (Fig. 1a) and distributed poloidally, as shown in Fig. 1b.

The wires of each thermocouple are spot-welded to the bellows

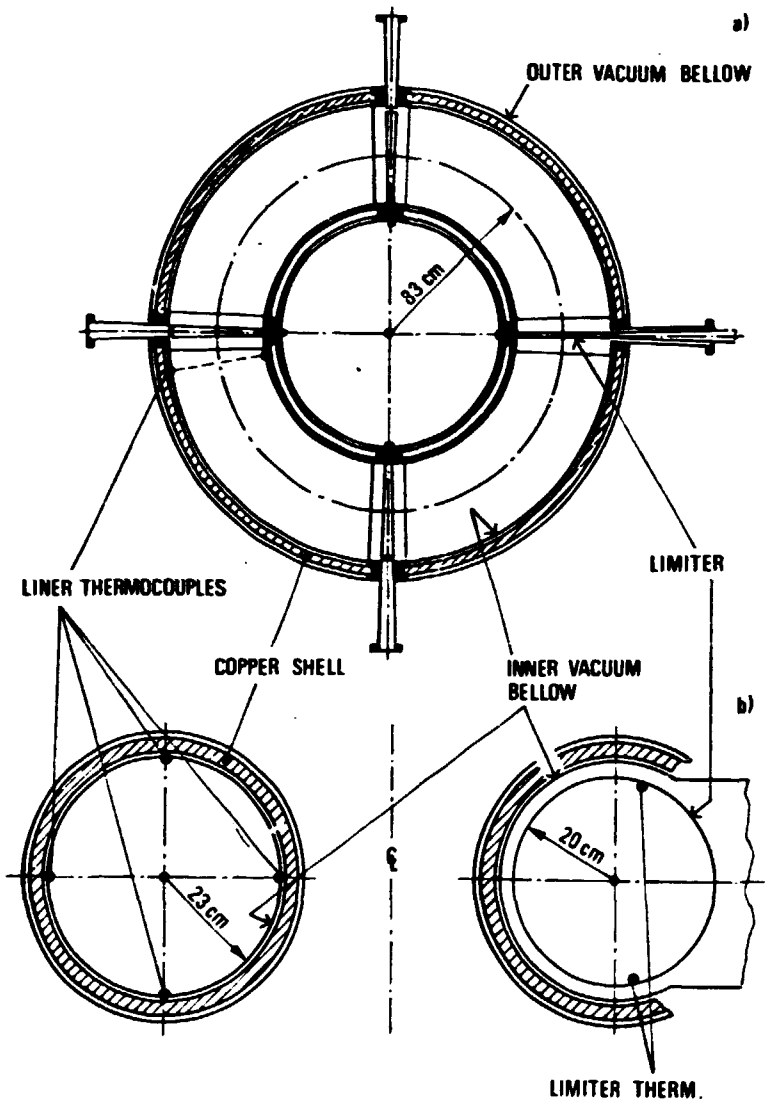

Fig. 1 a) General view of the FT vacuum chamber and toroidal location of thermocouples; b) poloidal location of thermocouples

separately so that the electrical connection is made through the bellows. This ensures that the temperature recorded is actually the temperature at the back surface of the bellows.

As already reported [3], the main poloidal limiter is monitored with two thermocouples.

These thermocouples are brazed at the center of the mushroom head at about 5 mm under the surface.

The poloidal location is about ± 80° from the midplane in the outer part (Fig. 1b).

The location was chosen according to the analysis of the previous limiter [1,2].

The zones chosen, in fact never showed damages which could be attributed to abnormal operating conditions (runaways, disruption, or plasma quench.

3. EXPERIMENTAL RESULTS

Two different limiters were used in 1985, both monitored with thermocouples. During this period, different types of discharges having a large variety of plasma parameters (B_T = 6 - 8 T; I_p = 250-550 kA; $\bar{n}_e = (0.3 - 3)\cdot 10^{14}$ cm^{-3} were effected on the FT. The discharges were either ohmic or RF heated. The RF power was always within 10% of the total input power.

The thermal responses of the thermocouples are not on the acquisition system of FT. Therefore, at different periods, the temperature increase of both the liner and the limiter was monitored. In order to examine an average feature, the measurements of the liner and limiter were performed either simoultaneously, or separately for different discharges.

About 200 stationary discharges (duration $\geq$ 1 sec; no poloidal asymmetries among thermocouples) were collected.

Figures 2 and 3 report the maximum temperatures measured on the limiter and liner as a function of electron density for different plasma current ranges.

On the limiter, an almost linear dependence of energy deposition on bulk electron mean density was confirmed [3,4].

The energy deposited on the liner shows a dependence on the bulk electron mean density and on the plasma current.

For plasma current lower than 450 kA, the energy absorbed on the liner increases with density up to $\bar{n}_e = 1.5\cdot 10^{14}$ cm^{-3} and than reaches a steady value or even decreases. A similar trend was inferred from bolometric measurements in Alcator A at a lower plasma current [5].

For higher plasma currents (> 450 kA), the energy absorbed on the liner increases with the electron density and, in the range we were able to examine, no saturation value was found.

4. POWER BALANCE

Among the discharges examined, we measured simoultaneosly the thermal response of both the liner and the limiter for 40 discharges in order to evaluate the power flowing to the limiter in the plasma edge region and the power which diffuses to the the wall.

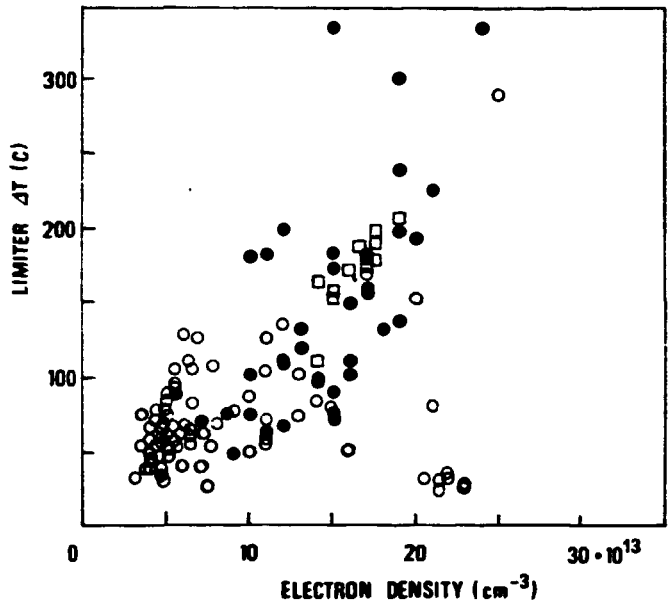

Fig. 2 Maximum temperature rise of the limiter mushroom heads.
(○ I_p = 250÷350 kA, ● I_p = 350÷450 kA, □ I_p = 450÷550 kA)

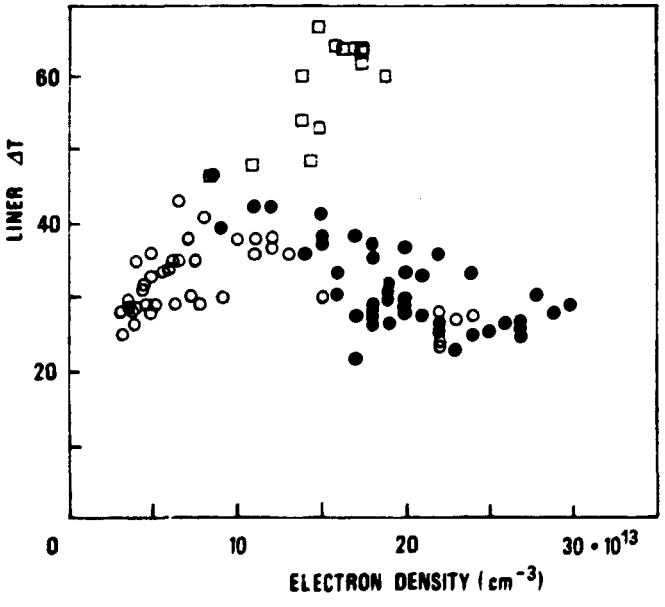

Fig. 3 Maximum liner temperature increase (○ I_p = 250÷350 kA, ● I_p = 350--450 kA, □ I_p = 450÷550 kA)

4.1. Power onto the limiter

As already known [6,7], the shape of the temperature increase versus time in a fixed point after a heat pulse is related to the characteristics of the pulse and to the physical properties of the material itself. The time at which the temperature reaches a fraction of the maximum temperature attained in the material does not depend on the total amount of energy absorbed.

The temperature history of the thermocouples in the limiter was calculated using the finite differences heat conduction code, HEATING 5, originally developed at Oak Ridge Nat. Lab [8], which was modified in order to consider a power flux due to conductive plasma losses exponentially decreasing in the scrape-off layer (SOL)

$$P(r,t) = P_o(t) \exp(-r/\lambda) \quad , \tag{1}$$

where r is the radial distance in the SOL; λ is the energy characteristic decay length; $P_o(t)$ is the power flux at r = 0. We found that the time variation of the power during the discharge does not change the shape of the temperature increase. On the contrary, the deposition radial profile plays a role in the shape of the temperature increase.

An energy decay length λ ranging from 0.5 to 1 cm was found to fit all the discharges examined with an average value near to the lower limit, in satisfactory agreement with the value inferred from Langumir probes [9] and molten layer thickness measurements [2].

The total power flowing to the limiter in the plasma edge region was calculated assuming that the energy flux is deposited over the effective area of the limiter without poloidal asymmetries and assuming a mean average value of λ = 1 cm.

A systematic over estimate of the power flux to the limiter can be deduced.

The total power flowing to the limiter ranges between 10% and 35% of the total input power, as shown in Fig. 4.

4.2 Power onto the liner

The heat flux to the liner was calculated using the a forementioned code, although the liner geometry should allow the use of the simple relation (which does not take into account boundary losses):

$$Q \; (\equiv \langle P \rangle \cdot \tau) = \rho \cdot c_p \cdot \ell \cdot \Delta T_M \quad , \tag{2}$$

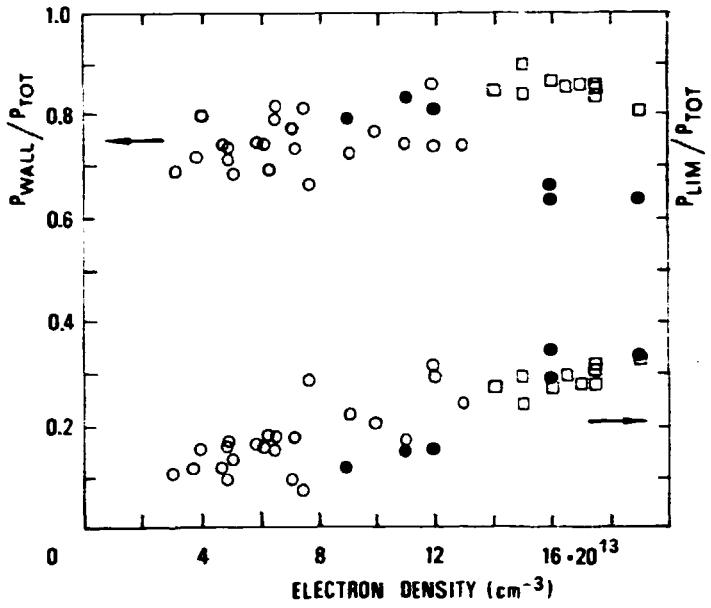

Fig. 4 Calculated fraction of the total power lost to the limiter and to the wall with respect to the total input power

where τ is the discharge duration; ρ is the material density; c_p is the specific heat; ℓ is the liner thickness; and ΔT_M is the maximum temperature increase.

The total power reaching the wall (radiation and change-exchange neutrals was calculated assuming a uniform deposition. The values, reported in Fig. 4, show that this represents a fraction of the order of 70% of the total input power, which increases if the electron density is increased with higher plasma current.

5. CONCLUSION

In the range of the errors due to the code simulation and to what has been assumed, the experimental data suggest a general feature of the power losses to the limiter and to the wall:

1)The power to the limiter shows an increase with increasing bulk electron density;

2)The power lost to the wall increases if the bulk electron density is increased with higher plasma current;

3)The overall energy balance seems to reach 100% of the total input power for $\bar{n}_e > 10^{14}$ cm^{-3} and higher plasma current suggesting a more uniform

deposition of the power to the limiter and to the wall. At lower density there is a systematic deficiency in energy balance and a large spread in experimental data, probably due to the presence of large poloidal and toroidal asymmetries.

REFERENCES

[1] C. Alessandrini, C. Ferro and M. Samuelli, Proc. 11th Symp. on Fusion Technology, Oxford (1980) 1067

[2] C. Ferro, G. Maddaluno, J. Nucl. Mater. 128&129 (1984) 822

[3] C. Ferro, et al., Proc. 12th European Conference on Controlled Fusion and Plasma Physics, Budapest 9F, 2 (1985) 555

[4] B. Lipschultz et al., J. Nucl. Mat. 128&129 (1984), 555

[5] L.S. Scaturro, M.M. Pickrell, Nucl. Fusion 20, 5 (1980), 527

[6] H.S. Carslaw and J.C. Jaeger, Conduction of Heat in Solids, Oxford University Press, New York, (1952) 2nd Ed.

[7] J.A. Cape, G.W. Lehman, J. Appl. Phys. 34, 7 July 1963, 1902 et related articles.

[8] W.D. Turner, D.C. Elrod, I.I. Simon-tov, ORNL/CSD/TM-15 (March 1977)

[9] V. Pericoli-Ridolfini, Plasma Phys. and Contr. Fusion, 27 (1985) 493

ACTIVATION AND DAMAGE BY RUNAWAY ELECTRONS ON FT LIMITER

G. Maddaluno, A. Vannucci*

Associazione EURATOM-ENEA sulla Fusione, Centro Ricerche Energia Frascati
C.P. 65 - 00044 Frascati, Rome (Italy)

ABSTRACT

Activation and metallographic analyses have been used in order to characterize the runaway electron interaction with the stainless steel limiter of the FT machine. Electrons with energy up to 20 MeV are found to hit the limiter with an average scrape-off length ranging from 0.05 to 0.1 cm. For an incidence time of 50 msec a power load $\geq$ 12 kW/cm^2 is deduced from the depth of the molten layer.

---

* ENEA Guest

1. INTRODUCTION

High energy electrons decoupled from the bulk of the plasma ("runaway" electrons) can cause heavy damage to the limiter in a tokamak machine [1-4].

Energy deposition is localized in a small area so that the heat load can reach dangerous levels with melting and vaporization of the limiter material. Moreover, the hard x-rays emitted by bremsstrahlung when runaways hit the limiter induce nuclear reactions leaving in turn a residual radioactivity in the limiter itself [2,5].

Nowadays, low runaway fluxes are obtained with a careful control of the discharge. Neverthless, they could represent a potential danger for long-life limiter operation in future machines.

The aim of this work is to characterize the limiter damage and activation by runaways in FT (Frascati Torus), within a larger program of plasma-limiter interaction study.

Information about runaway energy, radial penetration in the limiter scrape-off, and material damage are inferred. Some design consideration for the FTU (Frascati Tokamak Upgrade) limiter are discussed.

2. LIMITER DAMAGE BY RUNAWAY ELECTRONS

An AISI 316 stainless steel (recently also Inconel 600) poloidal limiter is used in FT [6]. The minor radius is 20 cm and the toroidal extension 2.8 cm. Since May 1983 the limiter has been equipped with 38 mushroom-shaped pieces tightened to a supporting structure.

Damage by runaway electrons on the FT limiter is concentrated in a region about 40° wide, centered around the outer mid-plane. Erosion and melting of the material are observed, located at the top of the mushroom surface.

The measured weight losses of the most damaged mushrooms for three different limiters used on FT are shown in Fig. 1. Material erosion is seen to have a maximum slightly off-centered bottomwards with respect to the mid-plane.

The same feature can also be recognized in all the limiters used in FT as far as the molten area is concerned, and probably is to be related to a systematic vertical displacement of the plasma column.

The fact that the more recent the limiter is the less the weight losses are, despite the number of shots, points out the achievement of an ever better control of the runaway fluxes during FT discharge.

3. ACTIVATION ANALYSIS

In order to get information about the energy of the runaway electrons, the outer part of the stainless steel limiter used in FT during a four months' period, from June to October 1984 (limiter IV in Fig. 1) was analyzed with a HPGe detector a few days after removal of the limiter.

The limiter had suffered about 800 low and high density deuterium discharges with both ohmic and LH radio frequency heating.

Typical main plasma parameters were I_p = 300 kA, B_T = 6-8 T, discharge duration ~ 1 sec. Eight discharges exhibited a very high hard-x-ray signal.

The extension of the activation was about 20° up and down the equatorial plane and coincident with the area of macroscopic damage.

From the γ-energy spectrum, five main radionuclides were reliably identified (^{57}Co, ^{54}Mn, ^{58}Co, ^{51}Cr, ^{56}Co) to be ascribed to (γ,n) or (γ,p) type processes, with a threshold energy ranging from ~ 8 to ~ 20 MeV.

As for weight loss measurements, the FT limiter configuration allowed the activation poloidal distribution to be measured for each radionuclide. A Gaussian-like distribution nearly centered around the midplane was found with a poloidal width decreasing with the increase of the energy threshold (Fig. 2). The mass losses suffered by the mushrooms were roughly taken into account as a weighting factor, with the depth of the activation region as the main uncertainty. No sampling in depth was made to avoid a long handling of the activated material.

4. METALLOGRAPHIC ANALYSES

Metallographic cross sections of the outermost mushrooms of the limiter used from October 1983 to January 1984 (limiter II in Fig. 1) had previously been made to characterize the thermal load by runaways with respect to the load by thermal plasma.

The mushrooms were cut parallel to the toroidal direction. Deep erosion radially extending up to ~ 3.5 mm from the top of the convex surface was noticed on the mushrooms closest to the equatorial plane corresponding to the weight losses reported in Fig. 1. Farther from this plane, mushroom cross sections showed a deep molten layer. In particular, a melt depth of ~ 1.2 mm as measured from the original surface was found on a mushroom located at the boundary of the damaged region, which could, in principle, be due to a single impact event. Much less deep molten

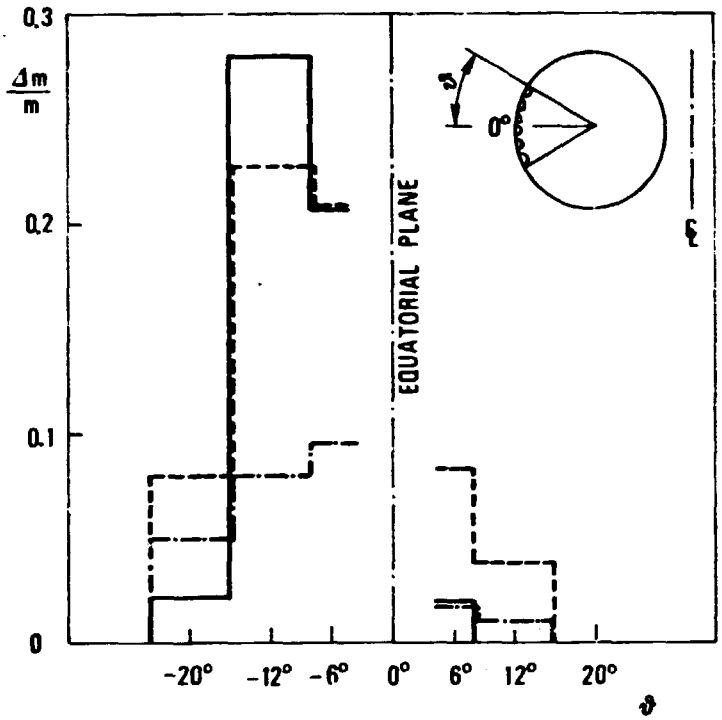

Fig. 1 Weight losses in the outer part of three FT limiters (— limiter II, 643 shots; --- limiter IV, 803 shots; – · – limiter VI, 520 shots).

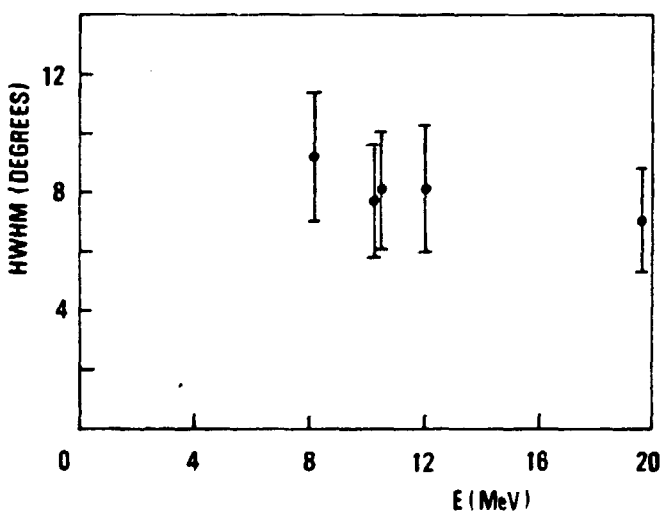

Fig. 2 Half-width half-maximum of the activation poloidal distribution as a function of threshold energy. The bars reflect the poloidal resolution of the measurement.

layers on the electron and ion side could be related to thermal plasma fluxes as found in regions fo the limiter not involved in runaways or disruptions [6].

5. DISCUSSION

The decrease of the activation distribution poloidal width with the increase of the electron energy suggested that a simple drift orbit model [7] could be applied in order to obtain information about the radial penetration of the runaways into the limiter scrape-off.

The radius of the runaway orbit just intersecting the limiter was calculated as a function of the runaway energy for a typical plasma current I_p = 300 kA and a realistic peaked current profile.

From geometrical considerations the roughly ± 20° wide activation distribution can be explained by assuming an average radial penetration of the runaway orbits into the limiter scrape-off ranging from 0.14 to 0.33 cm, in reasonable agreement with the findings from the metallographic analyses. Allowing for an exponential radial distribution of the runaway fluxes, an average e-folding length ranging from ~ 0.05 to ~ 0.1 cm was deduced.

The value of runaway electron energy inferred from the activation analysis was then used for calculating the energy deposition by fast electrons in a semi-infinite absorber [8].

The energy deposition profile in AISI 316 for two electron energies and for normal incidence is shown in Fig. 3. Energy appears to be deposited deeply in the inside of the material with a maximum at a depth increasing with the electron energy.

Therefore, as suggested by Nishikawa et al. [4], the surface energy deposition model used for limiter heating by thermal plasma cannot be applied. A simple heat conduction equation for volumetric heat generation in a surface layer of a semi-infinite volume was used to get the temperature rise of the limiter [9,10].

According to this equation, the temperature at depth x and at time t of a material with thermal diffusivity D, thermal conductivity k, due to a body heating in a thickness ℓ, is given by

$$T(x,t) = \frac{2DA_o t}{k} \left[1 - 2i^2 \operatorname{erfc}\left(\frac{\ell-x}{2\sqrt{Dt}}\right) - 2i^2 \operatorname{erfc}\left(\frac{\ell+x}{2\sqrt{Dt}}\right)\right] , \qquad (1)$$

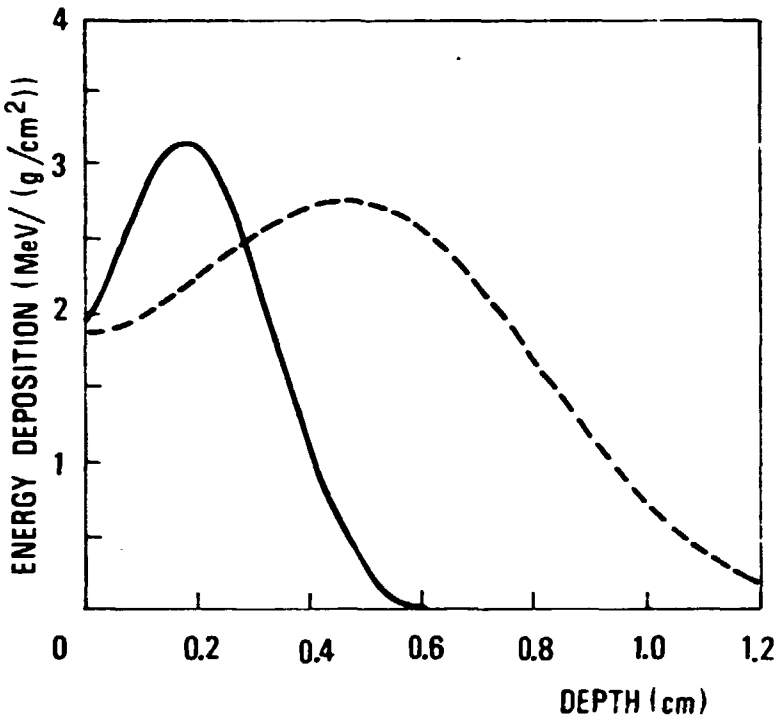

Fig. 3 Energy deposition profile for 8 MeV (solid line) and 20 MeV (dashed line) electrons within AISI 316 stainless steel at normal incidence.

where A_o is the volumetric rate of heat generation and i^2 erfc is the second integral of the complementary error function.

Several assumptions had to be made concerning the power load by runaways, the influence of the mushroom surface profile, and the boundary conditions.

An incidence time τ of 50÷100 msec, an average incidence angle of ~ 70° with respect to the normal, no radiation at the front surface, and an initial limiter temperature of 150°C were assumed.

Owing to the lack of temperature measurements in this part of the limiter [11], the heat conduction equation was tentatively used to explain the results of metallographic analyses. A power load $\geq$ 12 and $\geq$ 5 kW/cm^2 for τ = 50 and 100 msec is to be allowed in order to explain the amount of molten material.

6. CONCLUSIONS

Activation and metallographic analyses on the outer part of the FT limiter which is subject to runaway bombardment show that electrons of an energy as high as 20 MeV are created in the FT tokamak.

Such measurements integrated over a large number of shots allow only very global information on the runaway behaviour to be obtained. Moreover, the drift orbit model is a too simplified way to reproduce the actual situation in a tokamak discharge, and the phenomena affecting the runaway radial shift, such as magnetic turbulence [12], should be taken into account.

In any case, the runaway scrape-off length, depth of energy deposition, and power load as deduced from these analyses can be used for the improvement of the FTU limiter design [13].

A carefully shaped surface profile should be used in the outer part in order to optimize the heat load by runaways having a much shorter scrape-off length with respect to thermal plasma.

The increase of the penetration depth of the electron energy in low-z materials [4] with the consequent relaxing of the thermal stress, and the high photo-thresholds of carbon and its short-life radio-isotopes, which make handling less problematic suggest that graphite could be the most suitable material to be used for the outer half of the FTU limiter.

REFERENCES

[1] A.M. Oomens et al., Phys. Rev. Letts. 36 (1976) 255.

[2] TFR Group, J. Nucl. Mat. 93&94 (1980) 203.

[3] S.A. Cohen, R. Budny, G.M. McCracken et al., Nucl. Fusion 21 (1981) 233

[4] M. Nishikawa et al., J. Nucl. Mat. 128&129 (1984) 493.

[5] C.W. Barnes, J.M. Stavely Jr, J.D. Strachan, Nucl. Fusion 21 (1981) 1469.

[6] C. Alessandrini, C. Ferro and M. Samuelli, Proc. 11th Symp. on Fusion Technology, Oxford (1980) 1067.

[7] H. Knoepfel and D.A. Spong, Nucl. Fusion 19 (1979) 785.

[8] T. Tabata and R. Ito, Nucl. Sci. Eng. 53 (1974) 226.

[9] H.S. Carslaw, J.C. Jaeger, Conduction of Heat in Solids, 2nd Ed. Oxrford University Press (1959).

[10] J.R. Easoz, R. Bajaj, Proc. 10th Symposium on Fusion Engineering Philadelphia (1982) 1008

[11] G. Maddaluno, C. Ferro, M. Ciotti, these Proceedings.

[12] TFR Group, EUR-CEA-FC-1198 (1983).

[13] Frascati Tokamak Upgrade, Report 82.49, Associazione EURATOM-ENEA sulla Fusione, C.R.E. Frascati, Italy (1982).

EROSION-REDEPOSITION AND IMPURITY TRANSPORT IN THE SCRAPE-OFF LAYER OF THE FT TOKAMAK

E. Franconi,

Associazione EURATOM-ENEA sulla Fusione, Centro Ricerche Energia Frascati, C.P. 65 - 00044 Frascati, Rome (Italy)

F. Brossa

Commission of the European Community, Joint Research Center, Ispra Establishment, Material Science Division, 21020 Ispra (VA) Italy

ABSTRACT

Impurity transport processes, particle and impurity fluxes in the scrape-off layer (SOL) of the FT machine have been studied by means of two graphite probes acting as catcher-targets. Targets are analyzed after 217 deuterium FT-discharges (68% flat-top discharges, 32% disruption shots, and 1 runaway shot) using SEM, SAES, and SIMS surface techniques. SAES and SIMS analyses indicate that the main metallic impurities are Cr, Mn, Fe and Ni. Weight-loss measurements of the graphite probes evidence that the erosion of each sample is greater than the redeposition of the metallic film. Impurity fluxes due mainly to disruptions, runaway electrons, or PDC processes were observed to range from $6.5 \cdot 10^{15}$ to $1.2 \cdot 10^{16}$ atoms/cm^2 · discharge on the ion-drift side, and from $7.3 \cdot 10^{15}$ to $1.1 \cdot 10^{16}$ atoms/cm^2 · discharge on the electron drift side, at an average distance of 21 cm from the center line of the plasma. The e-folding length λ_{imp} of the SOL for the impurity flux was also estimated to lie in the range $9.8 < \lambda_{imp} \leq 12.5$ cm.

1. INTRODUCTION

The mechanism responsible for the production of impurities and their behaviour in the boundary layers of tokamaks are still not well understood. The study of the plasma-limiter interactions, by means of collector probes exposed in the edge plasma followed by surface analysis, is routinely used in different machines [1,2,3,4]. The aim is to provide valuable information to understand the causes of impurity release and transport from the limiter, as well as limiter erosion and damages produced by the plasma. The knowledge of the nature of these processes provides the basis of controlling them, and so achieve plasma conditions which may allow ignition to occur.

Post-mortem surface analysis of all FT stainless steel limiters has been performed for years [5,6,7] in order to collect data on the impurity transport processes and particle fluxes in the scrape-off layer (SOL) of the FT machine. The main poloidal limiter was recently (July 1985) equipped with mushroom-like elements of Inconel 600, and four graphite catcher-targets inserted between the mushroom heads and the limiter structure of AISI 316 SS, as shown in Fig. 1. During discharges, heavy impurity generation is mainly produced by erosion due to sputtering, arcing, and evaporation of the plasma-facing components; during and after each plasma discharge, such impurities are redeposited on the probes.

Deposition probes mounted on the FT limiter structure in both the upper and the lower half poloidal limiter are made of graphite (ELLOR#8 - Le Carbonne - Lorraine). They have been exposed for 217 deuterium discharges (68% flat-top, 32% disruptions and 1 ranaway shot) in the Frascati Tokamak. The FT machine main parameters, during the shots considered here, were $B_T \sim 4\text{-}6$ T; $I \sim 250\text{-}450$ kA; $< n_{o,e} > \sim (0.2\text{-}2)\cdot 10^{14}$ cm^{-3}, discharge lengths 0.8÷1s, for both ohmic and RF additional heating discharges (LHRH) with RF power up to 200 kW.

2. SURFACES ANALYSES OF THE COLLECTOR PROBES

The graphite probes, exposed to plasma shots at an average distance of 21 cm from the center line of the plasma, are transported in air to the surface analysis equipment.

Initially, "weight-loss" measurements on both targets are performed by means of a Mettler UM-3 microbalance (sensitivity $\lesssim$ 0.1 μgr). A reference "weight-loss" measurement on a graphite sample, mounted on the

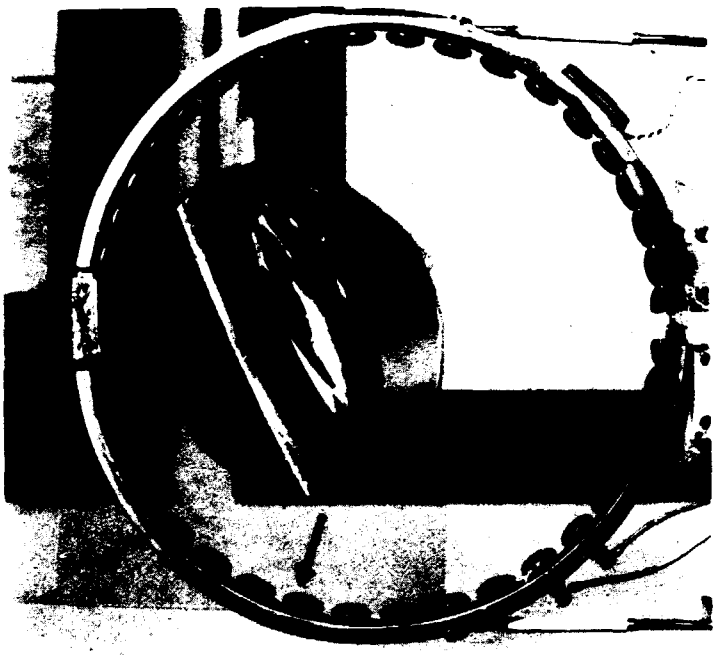

Fig. 1 Photograph of the FT limiter showing the 38 mushroom-like elements and both graphite catcher-targets analyzed (arrows). Particular of a graphite target as mounted on the limiter is also shown.

limiter but not exposed to the plasma, indicates that less than 2% of the weight change is due to the netting up of the probes.

The samples are then analyzed using a variety of surface analysis techniques (SEM, SIMS, SAES) in order to characterize the metal deposit on the probes. SEM analyses show that the redeposition of metallic impurities on the graphite targets (ion-drift side and electron-drift side) has three different features (Fig. 2):

- uniform atomic layers;
- material splashes from melting process;
- droplets, with diameters in the range of 0.1-10 μm.

Droplets on the graphite surface are expected beacuse of the agglomeration of redeposited films due to the surface tension of the metal heated up to melting point by both plasma current decay and local arcing [8].

Secondary ion mass spectroscopy (SIMS) was performed on the samples using a IMS3F-CAMECA with a raster facility for high lateral resolution which allow a deuterium depth profile with the best depth resolution [9].

Fig. 2 SEM micrographs of the metallic coating on the upper graphite-target after 217 tokamak discharges. a) general aspect; b) particular of droplets and metal splashes from melting process on the ion-drift side; c) splashed droplets on the electron-drift side.

The main SIMS experimental parameters were: rastered area 50x50 μm; an SI collection spot diameter 25 μm; C_s^+ primary ion current at 14.5 keV I_p ~ 0.55 μA. A typical SIMS spectrum of the metal layer is shown in Fig. 3, while the concentration of D in the layer has been measured as a function of the erosion time (minutes) in both the electron and ion sides (Fig. 4), together with Fe as metallic impurity. Subsequent profilometry measurements of the crater indicate that a depth scale for SIMS should be established with an accuracy of ±20%, assuming a mean erosion rate of 10 Å/s. The SIMS profile in Fig. 4 shows a different distribution between the ion and electron sides of the upper probe; in particular, a D-concentration peak of 1.3×10^4 c/s at a depth of 130 nm was found on the ion side. On the electron side, an exponential decay of deuterium in the target is observed. The 1/e fall-off, σ, in this profile results 30 nm for depths of less than 70 nm, and 120 nm for depths from 70 to 200 nm. However, any extrapolation to an absolute value of the D-conc requires additional tests with a calibrated standard marker. The deuterium distribution indicates that the net deposition in the ion side is mainly due to the D-trapping in the deposited impurity layer, which is strictly related to the heat flux distribution [10,11]. From our estimation, we find that the amount of deuterium trapped in the electron side is at least 15% lower than that in the ion side, and it remains in the layers also after removal from the vacuum vessel and exposure to the air. This exposure makes the metal deposit heavily oxidized, while the composition of the layers indicates the presence of Ni, Fe, Cr and Mn as metallic impurities (Fig. 3).

Sputter Auger Electron Spectroscopy (SAES) was carried out using a Perkin-Elmer mod. PHI-600 with a primary electron beam current of 0.3· μA, while the compositional depth profiles were performed using a 3 keV A_r^+ ion beam of I_p ~ 1 μA. From SAES analyses on both the ion and the electron sides (Fig. 5), the metal ratio of Ni/Ni+Fe+Mn+Cr concentrations shows that it corresponds to the mushroom-like element material, rather than to the SS of the liner and limiter structures. The total amount of impurities is calculated assuming an average atomic density of the layers of $8.5 \cdot 10^{22}$ atoms/cm^3. Table I reports the estimated average net deposition per discharge.

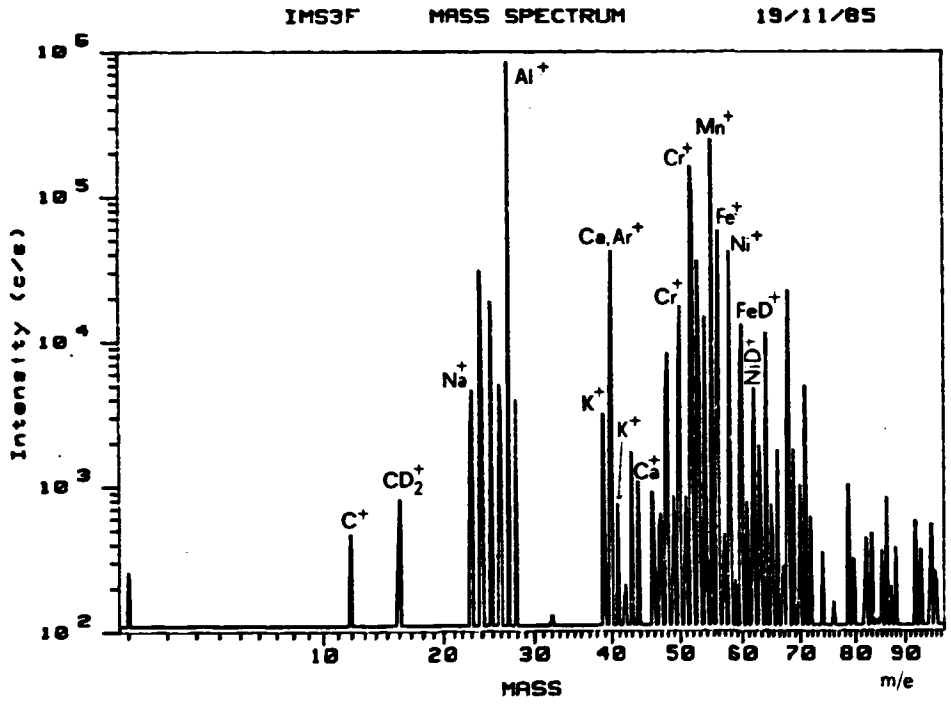

Fig. 3 SIMS spectrum of the graphite target coated with metallic layer after 217 tokamak discharges.

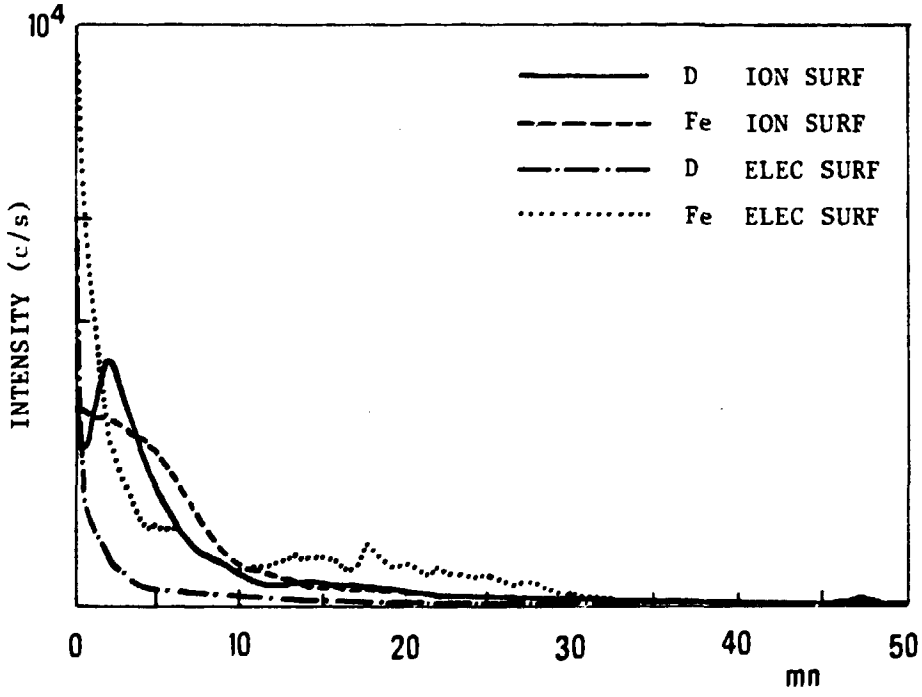

Fig. 4 SIMS depth profile of the metallized graphite target showing its D and Fe impurities content (ion and electron-drift side) after exposition to 217 plasma discharges as a function of the erosion time.

TABLE I

N_i average net deposition (atoms/cm^2 per discharge)·10^{15}

	Ion side	Electron side
Top $< r > = 21$ cm	12	7.3
Bottom $< r > = 21$ cm	6.5	11

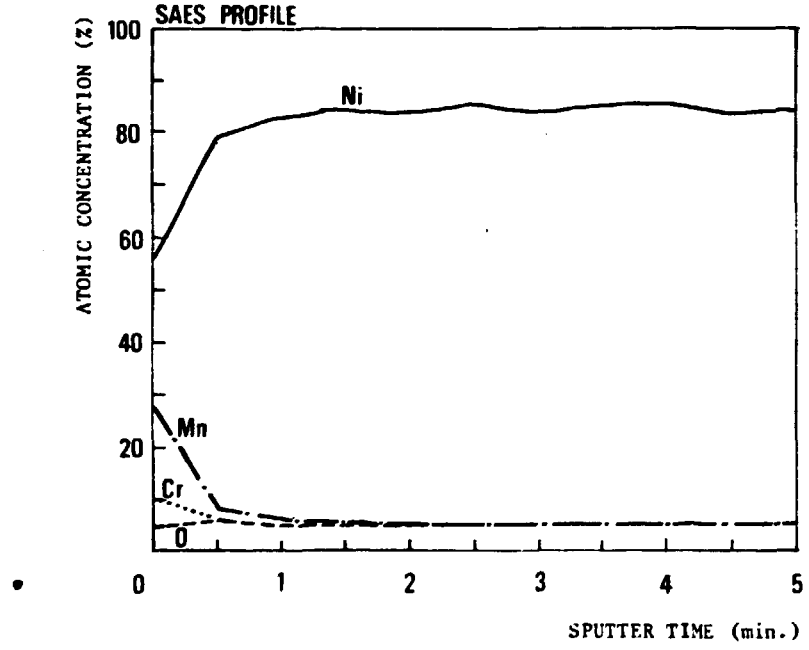

Fig. 5 SAES compositional depth profile of the redeposited metallic layer showing an atomic composition of 85% Ni, 5% Mn, 5% Cr, 5% O.

Both SIMS and SAES analyses confirm an asymmetrical behaviour of the heavy impurities deposition with respect to the meridian plane in directions parallel and antiparallel to the toroidal field, as already found for FT [7].

3. MECHANISMS OF IMPURITY PRODUCTION AND REDEPOSITION

The most significant light impurities in the plasma of the FT machine are always oxygen, and a minor quantity carbon and chlorine, resulting from water and hydrocarbon desorption from the wall and probably introduced into the torus by the detergent used for washing the limiter. Significant amounts of heavy impurities due to the erosion of the limiter

(mainly Mn, Fe, Cr, Ni) were found in the plasma, particularly at low n_e values, from spectroscopic measurements.

Weight-loss measurements performed on the graphite samples give $\Delta m_a \sim 2.1$ mgr and $\Delta m_b \sim 2.5$ mgr for the upper and lower half-limiter respectively. The net erosion of the graphite targets, i.e., sputtering, self-sputtering, evaporation and sublimation erosion, minus redeposition of heavy impurities indicates th t $\Delta m_{net} > \Delta m_{a,b}$ because

$$m_{Redep} = \Sigma_i A_i X_i \rho_i = A \cdot \bar{X} \cdot \bar{\rho} \geq 0.21 \text{ mgr} \qquad (1)$$

for each sample, according to the results of the SAES compositional depth profile. A_i, X_i, ρ_i and A, $\bar{X}$, $\bar{\rho}$ are respectively the area, thickness, and density of the redeposited metallic layer on the i-th point and averaged over all the area, A, by means of the SAES analysis. The compositional depth profile shows that the mean metallic thicknesses in both the top (T) and the bottom (B) parts of the ion and the electron sides are:

$$\bar{X}_{e,B} = 296 \text{ nm}; \ \bar{X}_{e,T} = 198 \text{ nm}; \ \bar{X}_{i,B} = 176 \text{ nm}; \ \bar{X}_{i,T} = 324 \text{ nm} \quad .$$

Even considering the lower limit for the redeposited amount of material, and a mean sputtering yield for graphite at 850° K by deuterium and carbon ions, i.e., $S_{(D,C\to C)} \sim 2.10^{-2}$ atoms/ion, deuterium and/or carbon fluxes in the SOL are found to range from 2.0 to $2.7 \cdot 10^{19}$ atoms/cm^2 · discharge, assuming on the edge of FT: $T_e \sim T_i$, $T_i \sim 20$ eV [12] $T_{imp} \sim 5$ eV for single-ionized C^+ atoms, as in other machines, hitting the probe at normal incidence [13,14,15].

In terms of fluxes, the net eroded flux is given by the difference between the sputtered, evaporated, and sublimated impurity flux and the redeposited flux:

$$\Gamma_z^E(A) = \Gamma_z^{SP}(A) + \Gamma_z^{VA}(A) + \Gamma_z^{SU}(A) - \Gamma_z^{RE}(A) \quad ; \qquad (2)$$

while the total redeposited flux on the surface A of the graphite target facing the plasma orthogonally to B_T is

$$\Gamma_z^{RE}(A) = \Gamma_{zp}(A) + \Gamma_{zl}(A) + \Gamma_{zD}(A) \quad , \qquad (3)$$

where Γ_{zp} is the material reaching the plasma from the limiter and returning, via diffusion, to the target surface, Γ_{zl} is the material from the limiter, ionized in the SOL, and returned to the target surface, and Γ_{zD} is the vapour-deposited material produced during disruptive events. Maximum net erosion by sputtering on the probe (limiter) seems to occur during the flat-top of the plasma current [6], while $\Gamma_z^{VA}(A)$ and $\Gamma_z^{SU}(A)$ reach their maximum during periods of MHD instability of the plasma (startup and shutdown) [16]. This result is in accordance with the Mn depletion on the AISI 316 SS surface due to the preferential evaporation found on the limiter surfaces by means of SEM-EDXA analyses [17], and with the frequent presence of a Mn-line peak at the beginning and end of the discharge [18].

At any radius $r > r_o$, where r_o = 20 cm (limiter radius), the net eroded flux Γ^E due to the ions during flat-top current is

$$\Gamma^E(r) = 1/2\ n_e(r_o)v_{sp}S_p e^{-r/\lambda_p} - 1/2\ \Sigma_j \gamma_j n_z(r_o)v_{szj}(1-S_{zj})\ e^{-r/\lambda zj} \quad , \qquad (4)$$

where v_{sp}; v_{szj}, S_{sp}, S_{zj}, λ_p, λ_{zj}; are the sound speed, sputtering yield, and e-folding length of the plasma and impurity ions, respectively; γ_j is the weight of each heavy impurity in the redeposited layer ($\gamma_{Mn,Cr}$ = 0.05, γ_{Ni}= 0.90 according to Fig. 5). If $\Gamma^E < 0$, a deposition-determined process occurs. Experimentally, it results that the catcher-area A of the probe a suffers an erosion-determined process, in fact:

$$\int_{r_1 r_o}^{r_2 - r_o} \Gamma^E(r)\ dr \simeq 7.2\cdot 10^{16}\ \left[\ \frac{\text{C-atoms}}{\text{cm}\cdot\text{s}}\ \right] \qquad ; \qquad (5)$$

where r_1 = 20.8 cm, r_2 =21.2 cm.

Furthermore, from the SAES depth profile performed on three different radial direction points of the a-probe (top) on both ion and electron sides, we get $\lambda_{Ni} = \lambda_{Mn,Cr} \sim 12.5$ cm on the ion-drift side and $\lambda_{Ni} = \lambda_{Mn,Cr} \sim 9.8$ cm on the electron-drift side so that the heavy impurity fluxes in the SOL are represented by

$$\Gamma^{RE}_{a,i}(r) = 1.5\cdot 10^{16}\ e^{-r/12.5} \qquad \Gamma^{RE}_{a,e}(r) = 9.5\cdot 10^{15}\ e^{-r/9.8}$$

These experimental λ-values take into account and impurity deposition

process occurring not only during normal steady state discharges but also during disruption conditions, so that exact λ-values can result different from measured values.

4. DISCUSSION

Assuming the plasma of the FT machine of circular cross section to be centered in the toroidal vessel, all the ions in the SOL hit the limiter, and most of them will be collected on it and can cause erosion by sputtering of the exposed surfaces. As a consequence, an impurity flux in the edge plasma composed of light and heavy ions with a different charge state takes place. The heavy impurity fluxes, detected by deposition probes at 0.8 cm from the plasma edge, do not necessarily represent the impurity efflux from the core plasma only, but rather seem to be a superposition of the core plasma impurity flux, with the local impurity flux originating from the limiter as the main additional source of heavy impurities. Because of the lack of data on toroidal and poloidal variations, local fluxes are extrapolated as impurity fluxes.

Asymmetrical behaviour of the limiter as a source of impurities [19] makes it difficult to estimate the impurity confinement time.

Synergistic effects, occurring at high temperature due to the ion and electron irradiation-induced reaction, which increase the graphite erosion are not taken into account because of the lack of appropriate data [20,21,22]. Large and undeep smooth craters observed on the bombarded graphite surface by stereomicroscope suggest that, in effect, a radiation--enhanced erosion mechanism takes place. Roth et al. [23] have shown that the high temperature erosion yield of graphite for incident H^+, D^+, and C^+ scales with the nuclear-deposited energy at the surface, and its maximum occurs between 700°K and 900°K, with a decrease of the deuterocarbon products concentration (CD_4) at higher temperature. This result indicates that a possible maximization of the chemical erosion coefficient on the probes may occur.

The collector flux $\Gamma_z^{RE}(A)$ was found to vary typically from $6.5 \cdot 10^{15}$ to $1.2 \cdot 10^{16}$ ions/cm^2 · discharge. Assuming that ions travel at 0.3 v_s, where v_s is the ion sound speed, for FT these fluxes correspond to a local impurity concentration of $3.2 \cdot 10^{12}$ cm^{-3} to 6.10^{12} cm^{-3}. These high impurity levels in SOL result greater than the levels found previously on FT [7]. A possible explanation is suggested by SEM observation: a combina-

tion of disruptive events, and microparticles emission (chunk) from the limiter should take place [6,8] during the late discharges which increase the "weight" of $\Gamma_{zD}(A)$ in $\Gamma_z^{RE}(A)$.

CONCLUSIONS

Experimental evidence integrated over a variety of discharge conditions of the FT machine leads to the conclusion that:

a) Chemical sputtering erosion of the graphite probes inserted on the FT limiter seems to occur. This erosion may increase for temperatures above 1300°K caused by a radiation-enhanced sublimation process on the target surfaces. On the contrary, physical sputtering appears to be less significant. A net deposition of deuterium with a peak on the ion side was also observed.

b) The evaluation of the impurity fluxes Γ_z^{SP}, Γ_z^{VA}, Γ_z^{SU}, Γ_z^{RE} by means of catcher-tagets and the measurement of $\Gamma^{RE}(A)$ are complicated because of their dependence on the radial and poloidal position of the collector probe, as observed in TFR-400 [24], and on the local asymmetries.

c) $\Gamma_z^E(A) > \Gamma_z^{RE}(A)$ demonstrates that the graphite targets are initially sputtered away, and then behave as a sink for metals.

d) The metal layers found as oxidized coating on the exposed surfaces have an atomic composition, indicating their main origin from the mushroom-like elements of the limiter. Furthermore, $\Gamma_z^E(A) > \Gamma_z^{RE}(A)$ suggests that these metal coatings are probably due to anomalous events, such as disruptionsor accidents, occurring at the last shots. Between #11527 and #11744 shots of FT, a mean erosion rate of $\sim 10^{20}$ C-atoms/s was evaluated from the sputtering ablation of impurities deposited on the graphite probes.

e) The impurity flux parallel to the magnetic field lines decays exponentially with a decay length $9.8\ \text{cm} \leq \lambda_{zj} \leq 12.5\ \text{cm}$, depending on the geometrical length of the flux tube in front of the catcher-probe.

f) The asymmetrical behaviour of the local heavy impurity source (limiter), in directions parallel and antiparallel to the toroidal field B_T supports the view that $\Gamma_z^{RE}(A)$ is strictly related to the non-ambipolarity of the plasma transport in the limiter shadow, which is justified by Nedospasov et al. [19], on the ground of the asymmetries in the sheath-potential.

ACKNOWLEDGEMENTS

Thanks are due to M. Barteri (C.S.M. - Roma), P. Delogu (ENEA TIB--MAT), M. Anderle (IRST - Trento) for performing SEM, SAES, and SIMS analyses respectively, and A. Neri for providing technical assistence. One of the authors (E. Franconi) is also indebted to Prof. B. Brunelli for his encouragement and Dr. L. Pieroni (FT Group) for many useful discussions.

REFERENCES

[1] G.M. Mc Cracken et al., J. Nucl. Mat 76&77 (1978) 431.

[2] W.R. Wampler et al., J. Nucl. Mat. 93&94 (1980) 139.

[3] M. Mohri et al., J. Nucl. Mat. 111&112 (1982) 147.

[4] G. Standenmaier, P. Staib, S. M. Rossnagel, J. Nucl. Mat. 111&112 (1982) 23.

[5] C. Ferro, E. Franconi, A. Neri, J. Nucl. Mat. 111&112 (1982) 573.

[6] E. Franconi, M. Barteri, G.M. Ingo, J. Nucl. Mat. 128&129 (1984) 481.

[7] C. Ferro, E. Franconi, et al., Proc. 12th European Conference on Controlled Fusion and Plasma Physic, Budapest 9F, 2 (1985) 555.

[8] E. Franconi, M. Barteri, G.M. Ingo, ENEA Report RT/FUS/84/4 (1984) 27.

[9] C.W. Magee, J. Vac. Sci. Technol. A1 (1983) 901.

[10] M. Braun, B. Emmoth, J. Nucl. Mat. 128&129 (1984) 657.

[11] S. Nagata et al., J. Nucl. Mat. 128&129 (1984) 760.

[12] V. Pericoli-Ridolfini, Plasma Physic and Controlled Fusion 27 (1985) 493.

[13] J. Roth et al., J. Nucl. Mat. 111&112 (1982) 775.

[14] J. Roth, J. Bohdansky and W. Ottenberger, IPP-Report 926 (1979).

[15] R. Yamada et al., J. Nucl. Mat. 95 (1980) 278.

[16] R.A. Zuhr et al., J. Nucl. Mat. 85&86 (1979) 979.

[17] E. Franconi, F. Brossa, P. Moretto, G. Rigon, Proc. of ICFRM-2, Chicago (1986) to appear on J. Nucl. Mat.

[18] G. Mazzitelli, Private communication.

[19] A.V. Nedospasov et al., Nucl. Fusion 25 (1985) 21.

[20] E. Vietzke, K. Flaskamp, V. Philipps, J. Nucl. Mat. 103&104 (1982) 673

[21] C.I.M. Ashby, R.R. Rye, J. Nucl. Mat. 103&104 (1981) 489.

[22] O. Auciello et al., Radiation Effects 89 (1985) 63.

[23] J. Roth, J.B. Roberto and K.L. Wilson, J. Nucl. Mat. 122&123 (1984) 1447.

[24] Equipe TFR, Proc. of the International Symposium on Plasma-Wall Interaction, Jülich, Pergamon Press (1977) 59.